THE JOURNAL OF PHYSICAL CHEMISTRY Letters

Letter

Cite This: J. Phys. Chem. Lett. 2017, 8, 5579-5586

pubs.acs.org/JPCL

Direct Mapping of Band Positions in Doped and Undoped Hematite during Photoelectrochemical Water Splitting

Andrey Shavorskiy,[†,▽] Xiaofei Ye,[‡] Osman Karslıoğlu,[†] Andrey D. Poletayev,[‡] Matthias Hartl,[†,#] Ioannis Zegkinoglou,[†,○] Lena Trotochaud,[†] Slavomir Nemšák,[†,◆] Claus M. Schneider,[§] Ethan J. Crumlin,[∥] Stephanus Axnanda,[∥,¶] Zhi Liu,[∥,&] Philip N. Ross,[⊥] William Chueh,[‡] and Hendrik Bluhm*[,†,∥]

[†]Chemical Sciences Division, Lawrence Berkeley National Laboratory, Berkeley, California 94720, United States

[‡]Material Science and Engineering Division, Stanford University, Stanford, California 94305, United States

[§]Peter-Grünberg-Institut-6, Forschungszentrum Jülich, 52425 Jülich, Germany

[∥]Advanced Light Source, Lawrence Berkeley National Laboratory, Berkeley, California 94720, United States

[⊥]Materials Sciences Division, Lawrence Berkeley National Laboratory, Berkeley, California 94720, United States

Supporting Information

ABSTRACT: Photoelectrochemical water splitting is a promising pathway for the direct conversion of renewable solar energy to easy to store and use chemical energy. The performance of a photoelectrochemical device is determined in large part by the heterogeneous interface between the photoanode and the electrolyte, which we here characterize directly under operating conditions using interface-specific probes. Utilizing X-ray photoelectron spectroscopy as a noncontact probe of local electrical potentials, we demonstrate direct measurements of the band alignment at the semiconductor/electrolyte interface of an operating hematite/KOH photoelectrochemical cell as a function of solar illumination, applied potential, and doping. We provide evidence for the absence of in-gap states in this system, which is contrary to previous measurements using indirect methods, and give a comprehensive description of shifts in the band positions and limiting processes during the photoelectrochemical reaction.

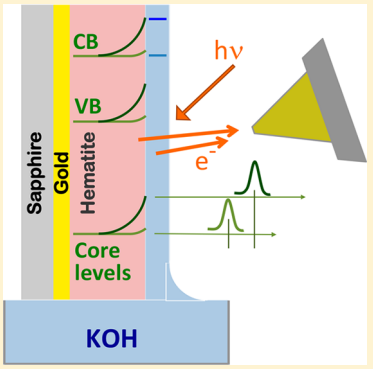

Since the first demonstration of an operating photoelectrochemical (PEC) cell in 1972,[1] economically viable and efficient water splitting has become an important yet still unreached goal.[2] One of the most significant obstacles for widespread use of this technology is the lack of photoanode materials that can operate in the harsh environment of a PEC cell.[3] Hematite (α-Fe_2O_3) is one of the most studied materials for the oxygen evolution reaction (OER) due to its chemical stability, low cost, and favorable band gap;[4] however, it has poor PEC performance. The PEC performance of hematite can be significantly improved by doping with, e.g., Ti,[5−15] but this does not solve the main problem for the limited hematite PEC efficiency, i.e., the large overpotential, which is commonly attributed to the sluggish OER kinetics and/or the fast recombination of photogenerated electron−hole pairs.[16−18] A number of recent studies focused on understanding the recombination process, in particular, the role of in-gap states. A commonly accepted scenario assumes that in-gap states act as trap centers for holes, thus preventing them from participating in the OER,[19] which in turn increases the probability for hole recombination with electrons. The trap states governing this mechanism are often attributed to Fe^{IV} surface intermediates[16,20−22] that are directly involved in the OER.[11,14,23−28] A recent attenuated transmission reflection infrared (ATR-IR) spectroscopy study[22] investigated the chemical composition of a D_2O/hematite interface during OER, showing the formation of ferryl iron species (Fe^{IV}=O), which were identified as hole trap states. The overpotential of the OER can in this case be decreased through the passivation of the surface states via growth of a thin oxide layer on the hematite surface[16,28−34] or their removal via annealing.[26] Recent evidence, however, indicates that surface states (which in this case could be electronic as opposed to molecular in nature)[25] play a less critical role in the recombination process;[17,18,33,35−38] the oxidation of water might instead occur through holes that are transferred directly from the valence band (VB) to the semiconductor surface, and the passivating oxide layer depletes electrons at the surface of the semiconductor, which results in a larger potential drop across the space charge region.[33,35] It should be noted that in the latter case the trap states might still exist in the band gap; however, they do not determine the PEC properties of hematite. Thus, although the two scenarios are not completely irreconcilable, the reaction intermediates and recombination mechanism are still under debate. In the

Received: September 26, 2017
Accepted: October 30, 2017
Published: October 30, 2017

DOI: 10.1021/acs.jpclett.7b02548
J. Phys. Chem. Lett. 2017, 8, 5579−5586

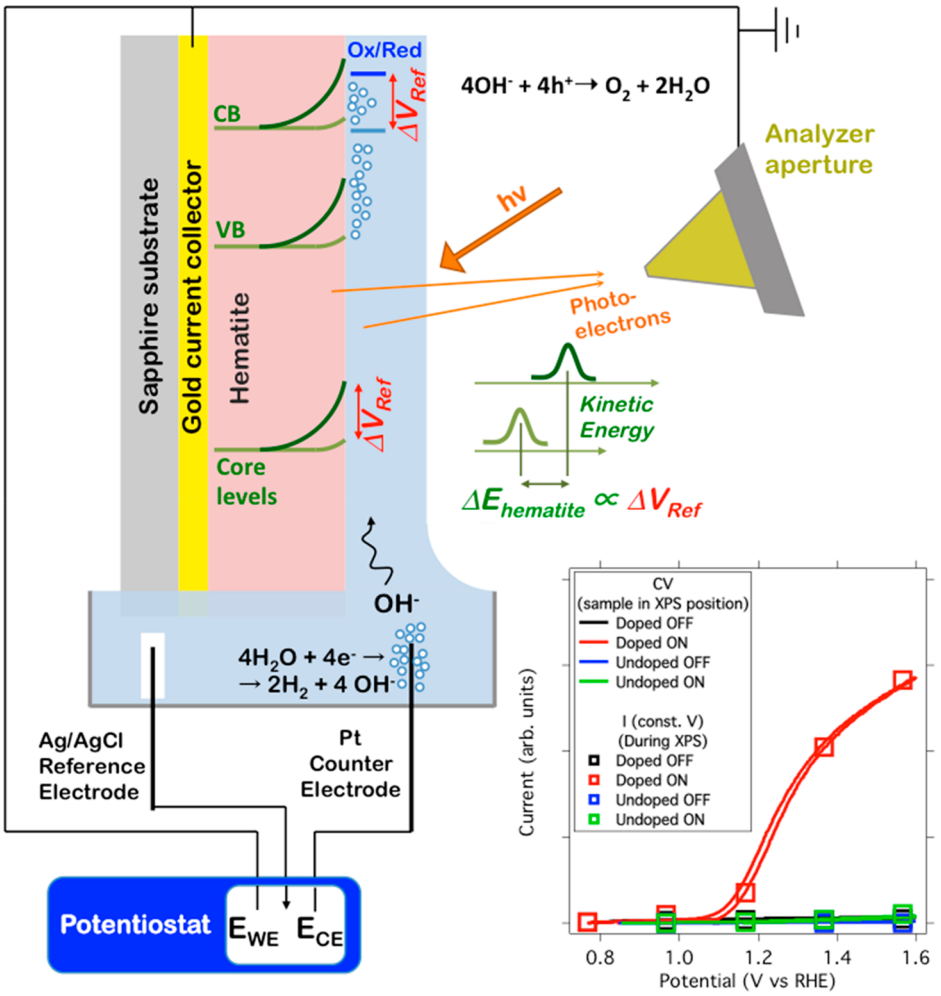

Figure 1. Measurement of band positions at the hematite/KOH interface. The hematite thin film (30 nm) sample is deposited on a gold current collector and is the working electrode in the system. A thin electrolyte thin film (10−20 nm) is prepared by dipping the sample into a beaker containing the solution of 0.1 M KOH and pulling it out slowly. The solution is in equilibrium with its vapor pressure (16−17 Torr) inside of a vacuum chamber. Photoelectron spectra are recorded using an ambient-pressure XPS system. Changes in the Ox/Red levels of the electrolyte (blue horizontal lines inside of liquid film) lead to analogous shifts (ΔV_{ref}) of the semiconductor band positions (green lines in the hematite film), affecting the measured kinetic energy of the electrons from the core levels (green peaks). A Pt counter electrode and Ag/AgCl reference electrode are used to control the potentials in the experiment. The inset shows cyclic voltammograms (CVs) and (constant V) current measurements recorded in the dark and under illumination for undoped and 5 atom % Ti-doped hematite, with the sample in the same position as in the APXPS measurements. The sweep rate for the CVs was 20 mV/s.

following, we describe direct measurements of the shifts in the band positions at the hematite/electrolyte interface, which allow a detailed description of the limiting processes during the PEC reaction at the hematite/electrolyte interface.

In the present study, we utilize *operando* ambient-pressure X-ray photoelectron spectroscopy to directly probe the energy level positions at the electrochemically active interface between intrinsic and doped hematite and a KOH solution under the influence of an external potential and simulated solar illumination (Figure 1). Changes in the energy level positions are detected by measuring the kinetic energy of the photoelectrons originating from the hematite/electrolyte interface, which provide an interface-specific and noncontact probe.[39,40] A flat and dense thin (30 nm) film of highly crystalline (5 atom % Ti)-doped hematite prepared by pulsed laser deposition (PLD; see the SI and ref 41) was used as a PEC anode. Figure 2a shows examples of O 1s spectra measured on a sample in contact with a thin 0.1 M KOH solution layer, prepared using the dip-and-pull method (see the Experimental Methods section and SI), as a function of illumination (black dots: light off; gray dots: light on) at potentials of 0.8 (bottom) and 1.6 V (top). All spectra show three peaks, assigned to hematite lattice oxygen ("hematite", apparent binding energy (BE) 529−530 eV), KOH solution ("solution", 532−533 eV), and water vapor ("H_2O_{vap}", 535−536 eV). The intensity of the hematite O 1s peak is comparable to that of the solution peak. This indicates the presence of a solution film with a thickness that is small enough to allow a noticeable portion of the photoelectrons (kinetic energy ≈ 2.6 keV) originating from the surface of the hematite to escape the solution, while the solution film is also sufficiently thick to maintain ionic contact with the bulk electrolyte, as verified by observing potential-dependent shifts of the solution O 1s spectra. Compared to the 0.8 V condition, a positive (anodic) potential causes a shift of all peaks toward an apparent lower BE. Solar illumination, on the other hand, leads to a smaller apparent BE shift at a potential of 1.6 V; no BE shifts are observed between light and dark conditions at 0.8 V. O 1s

DOI: 10.1021/acs.jpclett.7b02548
J. Phys. Chem. Lett. 2017, 8, 5579−5586

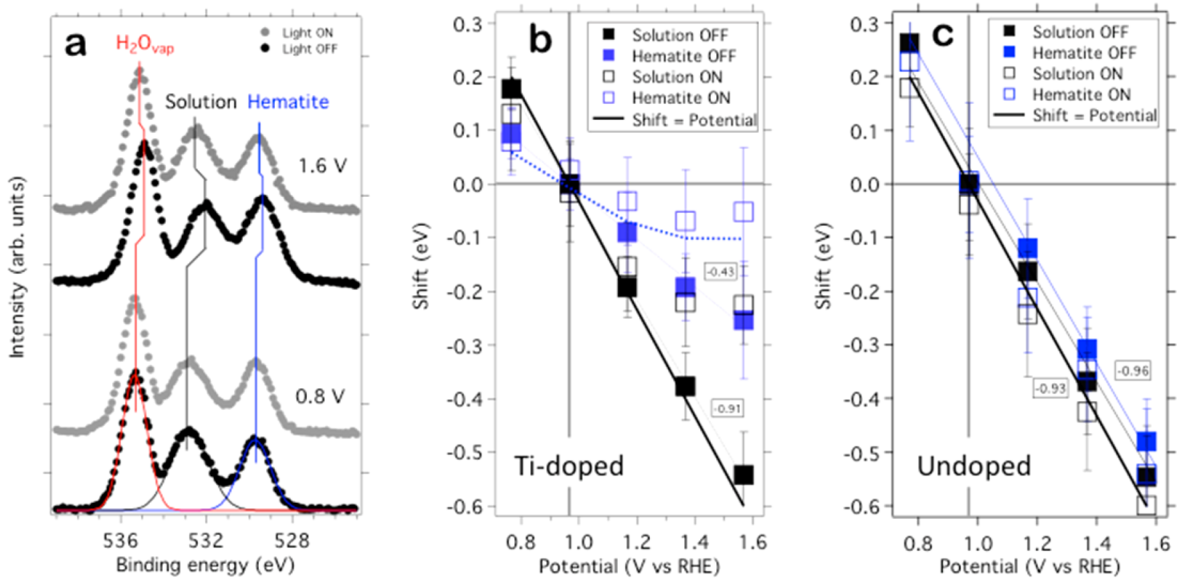

Figure 2. Oxygen 1s core level BE shifts as a function of potential, illumination, and doping. (a) O 1s photoelectron spectra of a 5 atom % Ti-doped hematite film at potentials *U* of 0.8 and 1.6 V. Experimental data in the dark (Light OFF) and under illumination (Light ON) are shown by black and gray markers, respectively. Lines represent fits to the data for the O 1s peaks of hematite (blue), 0.1 M KOH solution (black), and water vapor (red). (b) BE shifts of the solution (black) and hematite (blue) O 1s peaks. Filled (open) squares represent Light OFF (ON) conditions. The thin lines are linear fits to the data obtained in the dark. The thick black solid line has a slope of −1.0 as a reference for the case where the BE shift is equal to the applied potential. The dashed blue line indicates an estimate for the effect of the IR potential drop in the solution film under illumination on the BE shift of the hematite peak (see text). The error bars are defined as ±1 standard deviation and obtained from a statistical analysis of all measured BEs for a given experimental condition. (c) As in (b) but for an undoped hematite sample.

spectra were taken for a number of different potentials, ranging from 0.8 to 1.6 V. Higher potentials were not used due to the increased H_2 and O_2 production, leading to bubbling and possible spills into the electrostatic lens system of the electron spectrometer. The O 1s spectra are deconvoluted into three components for the hematite (oxide), solution, and water vapor (blue, black, and red lines, respectively, in the bottom spectrum in Figure 2a). The resulting BE shifts (after BE correction, Figure S1) are plotted as a function of applied potential and dark/light conditions for doped (Figure 2b) and undoped (Figure 2c) samples (see also Figure S7 for an additional data set). The shifts are referenced to the respective O 1s peak position at 0.964 V (0 V vs Ag/AgCl) in the dark. Shifts of the solution (oxide) peak BE are represented by black (blue) squares, where filled (open) squares indicate data obtained under dark (light) conditions. The thin lines are linear fits of the data. The thick solid black line indicates the trend line for the case that the BE shifts the same amount as the applied potential (slope −1.0). Under dark conditions the O 1s BE of the solution and oxide are linearly dependent on the applied potential for both doped and undoped samples. Under solar illumination, on the other hand, the BE shifts are similar to those in the dark for doped and undoped samples at low potentials but deviate from the linear trend observed in the dark at a potential above 1.2 V for the doped sample, while no significant difference for light vs dark conditions is observed for the undoped sample. The BE shifts observed in Figure 2 are unambiguously caused by changes in the applied potential. We can rule out any BE shifts due to changes in the chemical environment at the interface because we observe the same BE shifts for all measured core levels (O 1s: see Figure 2; Ti 2p, Fe 2p: see Figure S8). BE shifts caused by changes in the chemical environment would not be identical for the different core levels.

One striking observation that can be readily made from Figure 2b,c is the linear dependence of the hematite BE shift on the applied potential for both doped and undoped samples in the dark. On the basis of the framework of the Gerischer theory[42] (discussed below in more detail), this linear behavior indicates the absence of Fermi level pinning, which in turn is a strong indication for the absence of in-gap states in the potential range probed in these experiments, i.e., 0.4 to ca. 1.2 eV below the conduction band minimum (CBM) of hematite (Figure S2). Fermi level pinning would lead to the absence of BE shifts over a certain potential range where the in-gap (typically surface) states accommodate any charge flow across the interface; this was, for example, observed for the TiO_2/KOH interface.[43] In the case of band edge pinning (as opposed to Fermi level pinning), the semiconductor bands shift with the Ox/Red level of the electrolyte, resulting in a linear dependence of the apparent BE shifts of the semiconductor on the applied potential,[44] as observed in the present case of doped and undoped hematite in KOH. The absence of Fermi level pinning and/or in-gap states in our study is an intriguing observation and contrary to the findings in several recent reports, which indicated the presence of in-gap states between 0.4 and 0.9 eV below the CB of hematite (see Figure S2).[15,19,23,45] This difference could be attributed to several factors, such as the use of highly crystalline hematite in this study, which would suppress in-gap defect states at grain boundaries[46] or at the surface[15] or the formation of thin oxide overlayers[20] (e.g., passivation by a TiO_2 surface layer). However, several authors have pointed out that deep-lying trap states are intrinsic to hematite (e.g., oxygen vacancies originating from doping or nonstoichiometry)[45] and thus cannot be easily suppressed by the aforementioned factors. Our findings thus rather indicate that in-gap states are not always observed in doped and undoped hematite and that tunneling-mediated e^-/h^+

DOI: 10.1021/acs.jpclett.7b02548
J. Phys. Chem. Lett. 2017, 8, 5579−5586

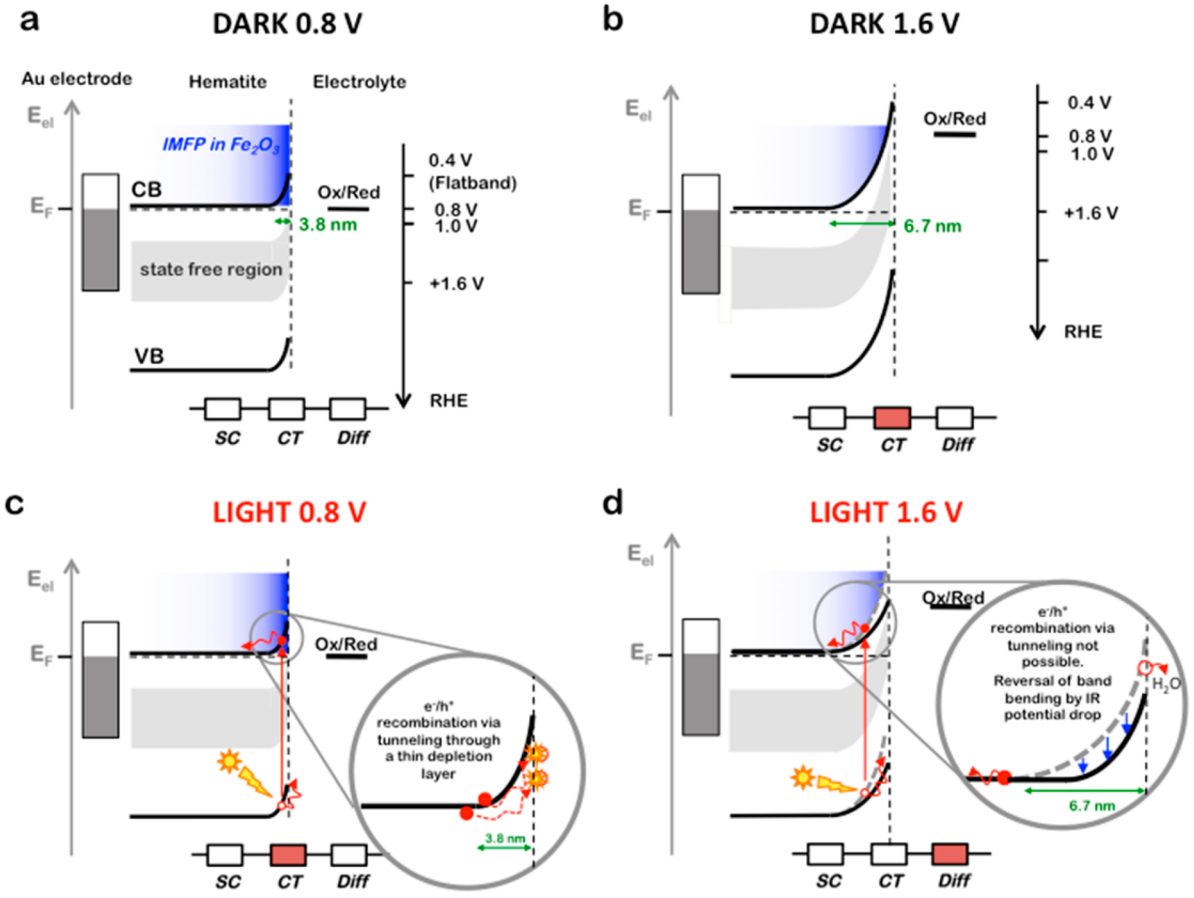

Figure 3. Changes in band positions in doped Fe_2O_3 under varying PEC conditions. Each diagram shows (from left to right) the position of the Fermi edge (E_F) in the Au substrate, the band positions in hematite, and the Ox/Red potential in the solution with respect to a reference electrode. The Au Fermi level is the reference level for electron energies in the system because the Au electrode is at the same potential as the electron energy analyzer. At the bottom of each diagram, an equivalent circuit diagram[11,14] is shown, with elements for processes in the space-charge region (SC), charge transfer (CT, i.e., OER reaction kinetics), and ion diffusion in the electrolyte (Diff), without capacitive elements for clarity. The process limiting the cell performance for each situation is shown in brick color. (a) Sample at 0.8 V in the dark. Because of the high doping level of hematite in this study, the CB minimum is close to E_F. Both CB and VB undergo upward band bending within the SCR (green arrow). The magnitude of the band bending and corresponding SCR width depend on the alignment of the bands and the Ox/Red potential of the electrolyte at the interface. (b) Same as (a) but at a 1.6 V potential. According to the data in Figure 2b, there is no Fermi level pinning, i.e., a change in the position of the electrolyte Ox/Red due to the applied potential leads to exactly the same change in the position of hematite band edges (here an increase in band bending). The absence of Fermi level pinning is indicated in all panels as a gray area below the CB, which shows the in-gap region, observed in the present experiments without any (in-gap) states. The limiting process at these conditions close to the onset of catalytic OER is charge transfer at the interface. (c) Sample at 0.8 V under illumination, which leads to the generation of electron−hole pairs that are spatially separated. Due to the narrow SCR, recombination through tunneling is efficient and no photocurrent is observed (see inset in (c)). (d) Sample at 1.6 V under illumination. The width of the SCR is increased compared to 0.8 V, and electron−hole recombination is less efficient, leading to generation of a photocurrent. The limiting process here is ion diffusion through the thin electrolyte film (Diff), leading to an IR drop of the Ox/Red potential at the hematite/electrolyte interface (gray vs black Ox/Red levels).

recombination is the most likely cause for the high OER overpotential. The relationship between in-gap states, electrode morphology, and processing conditions is currently being investigated.

On the basis of these observations, we now develop a comprehensive model for the change in the band position in the hematite anode as well as the shift of the redox levels in the solution using the framework of the Gerischer theory.[42] We first discuss the doped and undoped hematite samples under dark conditions (top row of Figures 3 and 4). At 0.8 V (Figures 3 and 4a), there is no net current flow in the system, and the Ox/Red level in the solution is aligned with the Fermi edge in the Au substrate, as is the CBM in the bulk of hematite. At the hematite/solution interface, the bands in hematite bend upward, which is characteristic for an n-type semiconductor.[4,42]

The magnitude of the band bending at 0.8 V is equal to the flatband potential of hematite, which we measured to be 0.39 V (Figure S3). When an anodic potential is applied to the working electrode (Figure 3b), the Ox/Red levels in the solution shift upward relative to the Fermi level of the Au contact and electron spectrometer by an amount equal to the applied potential. Such an effect has been previously observed for other semiconductor/liquid and metal/liquid systems[40,43,47,48] and indicates the absence of a potential drop across the thin liquid electrolyte film. Because there is no Fermi level pinning, the hematite band edges shift by the amount of the applied potential, causing an increase in band bending.

The most noticeable difference in the band energy diagram between doped and undoped hematite is the width of the depletion layer or space-charge region (SCR, green arrows in

DOI: 10.1021/acs.jpclett.7b02548
J. Phys. Chem. Lett. 2017, 8, 5579−5586

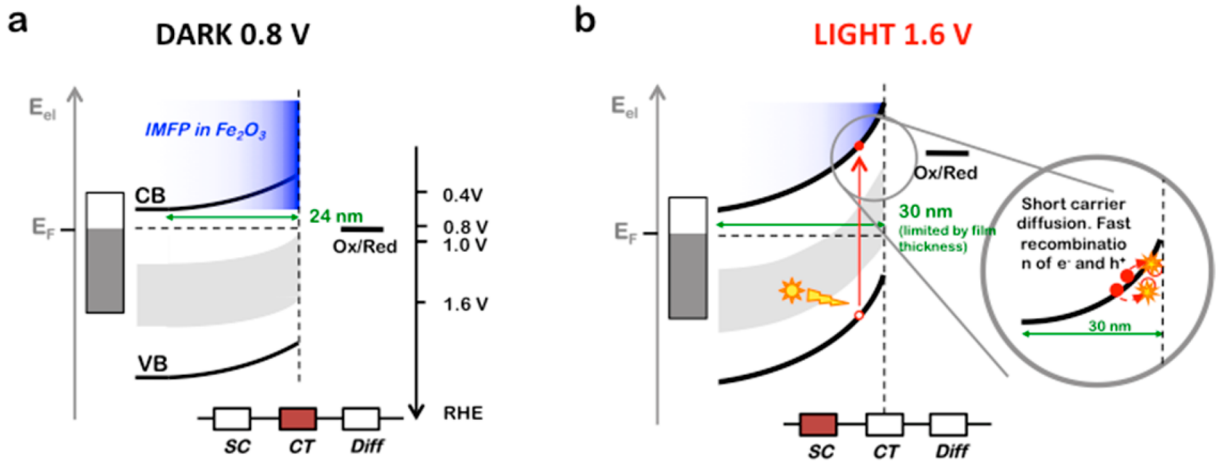

Figure 4. Changes in band positions in undoped Fe_2O_3 under varying PEC conditions. See Figure 3 for more details. (a) Sample in the dark at 0.8 V. Its Fermi level is 0−0.4 eV lower compared to E_F of the doped sample (Figure S2). The width of the SCR is substantially larger (24 nm) compared to that in doped hematite. (b) Sample at 1.6 V under illumination. The SCR width is now approaching the physical width of the hematite film, prohibiting the recombination of the photogenerated electron−hole pairs via tunneling. However, the low charge carrier concentration in undoped hematite limits the photocurrent due to the limited electrical conductivity in the solid.

Figures 3a,b and 4a), which is significantly smaller for the doped sample. The slope of the hematite O 1s BE vs potential dependence (−0.43 for doped and −0.96 for undoped sample) is in excellent agreement with the calculated slope (see Figures S4−S6) based on the effective electron inelastic mean-free path in hematite (5.3 nm), a dopant concentration of 1.6×10^{20} cm^{-3} for the doped and 3×10^{18} cm^{-3} for the undoped sample, and a flat band potential of 0.39 V, yielding depletion layer widths ranging from 3.8 (24 nm) to 6.7 nm (SCR comparable to a film thickness of 30 nm) for 5%-doped (undoped) hematite at 0.8 and 1.6 V, respectively. The strong deviation of the slope for doped hematite in the dark from the expected behavior (slope −1.0) is therefore not caused by a decreased band bending but rather a result of the convolution of the electron inelastic mean-free path and depth of the depletion layer, which are of similar values for the doped sample (Figure S5). On the other hand, depth-dependent changes in the potential distribution are less pronounced in the undoped hematite sample with a much wider depletion layer (Figure 4a and S5), leading to much smaller deviations from the ideal slope of −1.0 for the undoped hematite O 1s (Figure 2b,c) in the dark. Thus, both materials behave as ideal semiconductors, where the rate-limiting step is the kinetics of the OER (labeled CT in Figures 3 and 4).

We now turn our attention to the effect of illumination on the hematite/KOH interface, where doped and undoped hematite show substantial differences. In the case of undoped hematite, the effect of illumination is negligible: the BE shifts observed under illumination (open squares in Figure 2c) are identical to those observed in the dark (filled squares in Figure 2c) within the error bars. This implies equal bend bending for both cases and the absence of a surface photovoltage (Figure 3c,d). For an n-type semiconductor, a surface photovoltage (i.e., the result of the light-assisted creation of e^-/h^+ pairs and their subsequent separation at the semiconductor/electrolyte interface)[49,50] would lead to a decrease in band bending and consequently a positive BE shift, which is not observed for the undoped sample, indicating a very short carrier diffusion length, low majority carrier conductivity, fast e^-/h^+ recombination process, or a combination of these three factors (Figure 4b) as possible reasons for the low PEC activity.[7,10,11,46]

We now discuss the case of the doped sample under illumination. Here, two regimes can be distinguished, that of low potential and photocurrent (<1.2 V, Figure 3c), where the BE shifts in the dark and under illumination show similar behaviors (Figure 2b), and that of high potential/photocurrent (≥1.2 V, Figure 3d), where both hematite and solution O 1s peaks show a positive BE shift compared to the data measured under dark conditions. We note that the onset potential for the deviation between light and dark conditions coincides with the onset of the photoinduced OER reaction (∼1.2 V, CV in Figure 1). At low potentials (e.g., at 0.8 V), the overlap of the Light ON and OFF BE shifts is caused by the equal band bending in the semiconductor, similar to the case of undoped hematite. At higher potentials, however, illumination leads to an increase in the photocurrent, which in turn results in a limitation of the ion diffusion along the ultrathin electrolyte film, which is intrinsic to our measurement setup. This causes a potential drop $U = IR$ (with I as the photocurrent and R as the resistance of the liquid film) within the electrolyte solution layer and concurrent downward shift of the solution Red/Ox level (Figure 3d) and the semiconductor bands at the liquid/solid interface. The influence of this effect on the hematite BE was estimated by multiplying the BE shift of the solution under light illumination (open black squares in Figure 2b) by the ratio of hematite (blue filled squares) and solution (black filled squares) shifts in the dark (0.43). The resulting trend (dashed blue line in Figure 2b) represents the IR component of the light-induced hematite BE shift (blue open squares) and agrees well with the experimental data within the measurement error. This indicates that the effect of the surface photovoltage is negligible compared to the IR drop, most likely due to efficient e^-/h^+ recombination by tunneling through the narrow SCR in doped hematite (Figure 3c). A similar IR drop was also observed in our APXPS experiments at the KOH/Au interface (Figure S9) under catalytic OER conditions (e.g., above 1.7 V vs RHE). This implies that the observed potential deviation is indeed caused by an IR drop in the liquid film and not pinning of the Fermi level to depleted surface states because Fermi level pinning at the metal−liquid interface can be ruled out. Thus, in the absence of in-gap states, this is also the most probable reason for the large overpotential necessary for obtaining noticeable

DOI: 10.1021/acs.jpclett.7b02548
J. Phys. Chem. Lett. 2017, 8, 5579−5586

photocurrents, which require a sufficiently large width of the SCR to suppress tunneling and thus recombination of electrons and holes.

We also note that Fe 2p and Ti 2p spectra recorded for the highest and lowest potentials under dark and light conditions (see Figure S8) showed similar BE shifts as a function of potential and illumination as the hematite O 1s spectra, without any noticeable change in the peak shape. This supports the notion that the Ti dopants increase the hematite film conductance and that surface states do not play a significant role for charge transfer during the photoinduced OER.

The current findings and the proposed electron energy diagrams of the hematite/KOH interface provide evidence for a different model than that proposed in the literature,[19,23,24,26] including in a recent report[22] that suggested the existence surface trap states in the form of Fe^{IV}=O species under catalytic or light-assisted OER conditions. According to the impedance measurements in ref 22, these states appear at around 1.2 V vs RHE. We have conducted electrochemical impedance spectroscopy (EIS) on our samples under conditions similar to those in our XPS measurements (Figure S10). Qualitatively, the results from the doped sample agree well with the ones in ref 22—the capacitance of the surface states has a maximum at around 1.25 V vs RHE, although the absolute magnitude is an order of magnitude lower than that in, e.g., ref 18. The EIS data in Figure S10 as well as those in ref 22 provide no unambiguous indications for surface states. They can be explained based on the back electron−hole recombination process[17] and should not be interpreted as a defining spectral feature of the surface states without further evidence obtained using different methods.

The above discussion combined with the main spectroscopic observation of this study, namely, no Fermi level pinning over the potential range of 0.4−1.2 eV below the CB, leads us to conclude that surface states are absent in the hematite films in our study and the main recombination channel is back e^-/h^+ recombination. In this model, the ferryl irons reported in ref 22 could still be intermediates in the OER; however, they would not be energetically positioned between 0.4−1.2 eV below the CB. Alternatively, they could originate from oxidized iron species, caused by photoinduced corrosion of the hematite, similar to what has been observed for other semiconductors.[51−54]

In summary, our observations imply that (over the potential range used in this study) both doped and undoped hematite behave similar to ideal semiconductors, despite their substantially different carrier concentrations. The Ti-doped hematite film effectively conducts charge carriers, without noticeable bulk recombination losses, in agreement with previous theoretical simulations as well as experiments, contrary to the undoped hematite film (Figure 4b) where low charge carrier density and/or short carrier diffusion is the origin of the poor PEC activity. The absence of in-gap states for both doped and undoped hematite over a potential range of 0.4 to ca. 1.2 eV below the CBM (in contrast to previous findings) implies that surface states do not play a major role in mediating charge transfer and that tunneling-mediated e^-/h^+ recombination is the most likely cause for the large overpotential required for PEC oxygen evolution in hematite.

EXPERIMENTAL SECTION

Undoped and 5 atom % Ti-doped hematite films with a thickness of 30 nm were grown by PLD on a gold-covered sapphire crystal wafer (gold thickness ≈ 200 nm). The PLD (PLD/MBE-2300, PVD products) was done using a KrF (248 nm) excimer laser at fluence of 1 J/cm^2 and a repetition rate of 4 Hz. The deposition was performed at a sample temperature of 450 °C (infrared heater) and in 10 mTorr O_2. Prior to the measurements, the wafer was cut into 4−5 mm wide and 4−5 cm long strips. Physical characterization has been reported in ref 41.

APXPS experiments were performed at beamline 6.0.1 of the Advanced Light Source in Berkeley, CA, USA using a Specs Phoibos-NAP 150 hemispherical analyzer. X-rays from the beamline enter the chamber via a 100 nm thick Si_3N_4 window under ∼5° grazing incidence, and the photoelectrons are collected at a 40° emission angle. O 1s, Fe 2p, and Ti 2p XPS spectra were measured using an excitation energy of 3100 eV, which corresponds to a range of electron kinetic energies from ∼2700 to ∼2400 eV for the measured core levels. The predicted inelastic mean-free path of electrons with these energies is ∼8 nm, corresponding to ∼27 water layers.[55] The Fe 2p and Ti 2p showed the same BE shifts as the O 1s spectra as a function of potential and illumination, but otherwise, there were no discernible differences (Figure S8). C 1s and K 2p spectra were also recorded. In the majority of the experiments, a noticeable amount of both hydrocarbons and carboxylic species was observed at the interface between the electrolyte and the gas phase. For the analysis of the O 1s XPS data, a Shirley background was subtracted and the peaks were fitted with pseudo-Voigt line shapes.

The analysis chamber was equipped with a standard three-electrode electrochemical cell (Figure 1), consisting of a glass beaker (∼50 mL) containing 0.1 M KOH solution as well as a Ag/AgCl reference electrode and Pt counter electrode. The hematite sample was the working electrode and grounded to the spectrometer to ensure a common energy reference in all photoemission measurements. The electrochemical cell was controlled by a BioLogic SP-200 potentiostat. For the measurements under illumination, an Asahi Spectra solar simulator was used. All potentials mentioned in the text are referenced to RHE ($E_{RHE} = E_{Ag/AgCl}^0 + 0.059pH + E_{Ag/AgCl}$, $E_{Ag/AgCl}^0 = 0.197$ V, pH = 13), unless otherwise stated.

The sample was cleaned electrochemically inside of the EC cell by running several CV cycles (0.8 to +1.6 V, 20 mV/s) with the sample fully immersed in the KOH solution until no oxidation peaks associated with carbon-containing species were observed in the voltammograms. After the cleaning cycles, the sample was raised 10−20 mm in the presence of close to 100% relative humidity, such that the bottom part of the sample still maintained physical contact with the electrolyte. In such way, a very thin (about 10−20 nm thick) film of electrolyte remained on the surface of the sample several mm above the bulk solution level. This electrolyte film maintained electrical contact with the bulk solution. Typical CVs for doped and intrinsic hematite films measured with the sample in the XPS position are shown in Figure 1 with black (blue) lines representing sweeps under dark conditions and red (green) lines sweeps under illumination for the doped (undoped) sample. Static current (i.e., constant V) measurements taken during the APXPS measurements overlap with the dynamic CV data. Depending on the alignment of the solar simulator with respect to the sample, the photocurrent could be changed by a factor of up to 2.5 but did not influence the results of the APXPS data analysis.

DOI: 10.1021/acs.jpclett.7b02548
J. Phys. Chem. Lett. 2017, 8, 5579−5586

During the experiments, the pressure inside of the analysis chamber was maintained at 16−17 Torr. Watervapor pumped through the entrance aperture of the electron spectrometer was replenished from an additional water source, attached to the chamber. The change of electrolyte level in the glass cell was less than 1 mL in 12 h.

■ ASSOCIATED CONTENT

Supporting Information

The Supporting Information is available free of charge on the ACS Publications website at DOI: 10.1021/acs.jpclett.7b02548.

Binding energy and peak width determination, measurement of the impedance and dopant concentration, additional O 1s, Fe 2p, and Ti 2p data sets, and control experiment on Au foil (PDF)

■ AUTHOR INFORMATION

Corresponding Author

*E-mail: hbluhm@lbl.gov. Address: Lawrence Berkeley National Laboratory, Chemical Sciences Division and Advanced Light Source, One Cyclotron Road, Berkeley, CA 94720, USA.

ORCID

Lena Trotochaud: 0000-0002-8816-3781
Slavomir Nemšák: 0000-0002-6103-2925
Claus M. Schneider: 0000-0002-3920-6255
Ethan J. Crumlin: 0000-0003-3132-190X
Zhi Liu: 0000-0002-8973-6561
William Chueh: 0000-0002-7066-3470
Hendrik Bluhm: 0000-0001-9381-3155

Present Addresses

[▽]A.S.: MAX IV Laboratory, Lund University, Lund, 221-00, Sweden.
[#]M.H.: Physikalisches Institut, Universität Würzburg, Würzburg 97074, Germany.
[○]I.Z.: Department of Physics, Ruhr-University Bochum, 44780 Bochum, Germany.
[◆]S.N.: Peter-Grünberg-Institut-6, Forschungszentrum Jülich, 52425 Jülich, Germany.
[¶]S.A.: BASF Corporation, 25 Middlesex Essex Turnpike, Iselin, NY 08830, USA.
[&]Z.L.: Division of Photon Science and Condensed Matter Physics, School of Physical Science and Technology, ShanghaiTech University, Shanghai 200031, China.

Notes

The authors declare no competing financial interest.

■ ACKNOWLEDGMENTS

This work was supported by the Director, Office of Science, Office of Basic Energy Sciences, and by the Division of Chemical Sciences, Geosciences and Biosciences of the U.S. Department of Energy at LBNL under Contract No. DE-AC02-05CH11231. The Advanced Light Source is supported by the Director, Office of Science, Office of Basic Energy Sciences of the U.S. Department of Energy at LBNL under Contract No. DE-AC02-05CH11231. X.Y. and W.C.C. were supported by the Global Climate Energy Project at Stanford University. X.Y. was supported additionally by the Stanford Graduate Fellowship.

■ REFERENCES

(1) Fujishima, A.; Honda, K. Electrochemical Photolysis of Water at a Semiconductor Electrode. *Nature* **1972**, *238*, 37−38.
(2) Gratzel, M. Photoelectrochemical Cells. *Nature* **2001**, *414*, 338−344.
(3) Kudo, A.; Miseki, Y. Heterogeneous Photocatalyst Materials for Water Splitting. *Chem. Soc. Rev.* **2009**, *38*, 253−278.
(4) Walter, M. G.; Warren, E. L.; McKone, J. R.; Boettcher, S. W.; Mi, Q.; Santori, E. A.; Lewis, N. S. Solar Water Splitting Cells. *Chem. Rev.* **2010**, *110*, 6446−6473.
(5) Kronawitter, C. X.; Zegkinoglou, I.; Shen, S.-H.; Liao, P.; Cho, I. S.; Zandi, O.; Liu, Y.-S.; Lashgari, K.; Westin, G.; Guo, J.-H.; et al. Titanium Incorporation Into Hematite Photoelectrodes: Theoretical Considerations and Experimental Observations. *Energy Environ. Sci.* **2014**, *7*, 3100−3121.
(6) Glasscock, J. A.; Barnes, P. B. F.; Plumb, I. C.; Savvides, N. Enhancement of Photoelectrochemical Hydrogen Production from Hematite Thin Films by the Introduction of Ti and Si. *J. Phys. Chem. C* **2007**, *111*, 16477−16488.
(7) Hahn, N. T.; Mullins, C. B. Photoelectrochemical Performance of Nanostructured Ti- and Sn-Doped α-Fe_2O_3 Photoanodes. *Chem. Mater.* **2010**, *22*, 6474−6482.
(8) Kumari, S.; Singh, A. P.; Sonal; Deva, D.; Shrivastav, R.; Dass, S.; Satsangi, V. R. Spray Pyrolytically Deposited Nanoporous Ti^{4+} doped hematite thin films for efficient photoelectrochemical splitting of water. *Int. J. Hydrogen Energy* **2010**, *35*, 3985−3990.
(9) Wang, G.; Ling, Y.; Wheeler, D. A.; George, K. E. N.; Horsley, K.; Heske, C.; Zhang, J. Z.; Li, Y. Facile Synthesis of Highly Photoactive α-Fe_2O_3-Based Films for Water Oxidation. *Nano Lett.* **2011**, *11*, 3503−3509.
(10) Cao, D.; Luo, W.; Li, M.; Feng, J.; Li, Z.; Zou, Z. A Transparent Ti^{4+} Doped Hematite Photoanode Protectively Grown by a Facile Hydrothermal Method. *CrystEngComm* **2013**, *15*, 2386−2391.
(11) Miao, C.; Ji, S.; Xu, G.; Liu, G.; Zhang, L.; Ye, C. Micro-Nano-Structured Fe_2O_3:Ti/$ZnFe_2O_4$ Heterojunction Films for Water Oxidation. *ACS Appl. Mater. Interfaces* **2012**, *4*, 4428−4433.
(12) Shen, S.; Kronawitter, C. X.; Wheeler, D. A.; Guo, P.; Lindley, S. A.; Jiang, J.; Zhang, J. Z.; Guo, L.; Mao, S. S. Physical and Photoelectrochemical Characterization of Ti-doped Hematite Photoanodes Prepared by Solution Growth. *J. Mater. Chem. A* **2013**, *1*, 14498−14506.
(13) Fu, Z.; Jiang, T.; Liu, Z.; Wang, D.; Wang, L.; Xie, T. Highly Photoactive Ti-doped α-Fe_2O_3 Nanorod Arrays Photoanode Prepared by a Hydrothermal Method for Photoelectrochemical Water Splitting. *Electrochim. Acta* **2014**, *129*, 358−363.
(14) Mirbagheri, N.; Wang, D.; Peng, C.; Wang, J.; Huang, Q.; Fan, C.; Ferapontova, E. E. Visible Light Driven Photoelectrochemical Water Oxidation by Zn- and Ti-Doped Hematite Nanostructures. *ACS Catal.* **2014**, *4*, 2006−2015.
(15) Franking, R.; Li, L.; Lukowski, M. A.; Meng, F.; Tan, Y.; Hamers, R. J.; Jin, S. Facile Post-growth Doping of Nanostructured Hematite Photoanodes for Enhanced Photoelectrochemical Water Oxidation. *Energy Environ. Sci.* **2013**, *6*, 500−512.
(16) Barroso, M.; Pendlebury, S. R.; Cowan, A. J.; Durrant, J. R. Charge Carrier Trapping, Recombination and Transfer in Hematite (a-Fe2O3) Water Splitting Photoanodes. *Chem. Sci.* **2013**, *4*, 2724−2734.
(17) Le Formal, F.; Pendlebury, S. R.; Cornuz, M.; Tilley, S. D.; Grätzel, M.; Durrant, J. R. Back Electron-Hole Recombination in Hematite Photoanodes for Water Splitting. *J. Am. Chem. Soc.* **2014**, *136*, 2564−2574.
(18) Klahr, B.; Hamann, T. Water Oxidation on Hematite Photoelectrodes: Insight into the Nature of Surface States through In Situ Spectroelectrochemistry. *J. Phys. Chem. C* **2014**, *118*, 10393−10399.
(19) Klahr, B.; Gimenez, S.; Fabregat-Santiago, F.; Hamann, T.; Bisquert, J. Water Oxidation at Hematite Photoelectrodes: The Role of Surface States. *J. Am. Chem. Soc.* **2012**, *134*, 4294−4302.
(20) Takashima, T.; Ishikawa, K.; Irie, H. Fabrication and Characterization of Semiconductor Photoelectrodes with Orienta-

DOI: 10.1021/acs.jpclett.7b02548
J. Phys. Chem. Lett. 2017, 8, 5579−5586

tion-Controlled α-Fe_2O_3 Thin Films. *J. Phys. Chem. C* **2016**, *120*, 24827−24834.
(21) Yatom, N.; Neufeld, O.; Caspary Toroker, M. Toward Settling the Debate on the Role of Fe_2O_3 Surface States for Water Splitting. *J. Phys. Chem. C* **2015**, *119*, 24789−24795.
(22) Zandi, O.; Hamann, T. W. Determination of Photoelectrochemical Water Oxidation Intermediates on Hematite Electrode Surfaces Using Operando Infrared Spectroscopy. *Nat. Chem.* **2016**, *8*, 778−783.
(23) Klahr, B.; Gimenez, S.; Fabregat-Santiago, F.; Bisquert, J.; Hamann, T. Electrochemical and Photoelectrochemical Investigation of Water Oxidation with Hematite Electrodes. *Energy Environ. Sci.* **2012**, *5*, 7626−7636.
(24) Zandi, O.; Klahr, B.; Hamann, T. W. Highly Photoactive Ti-doped α-Fe_2O_3 Thin Film Electrodes: Resurrection of the Dead Layer. *Energy Environ. Sci.* **2013**, *6*, 634−648.
(25) Peter, L. M. Energetics and Kinetics of Light-driven Oxygen Evolution at Semiconductor Electrodes: The Example of Hematite. *J. Solid State Electrochem.* **2013**, *17*, 315−326.
(26) Zandi, O.; Hamann, T. W. Enhanced Water Splitting Efficiency Through Selective Surface State Removal. *J. Phys. Chem. Lett.* **2014**, *5*, 1522−1526.
(27) Du, C.; Zhang, M.; Jang, J. W.; Liu, W.; Liu, G.-Y.; Wang, D. Observation and Alteration of Surface States of Hematite Photoelectrodes. *J. Phys. Chem. C* **2014**, *118*, 17054−17059.
(28) Fu, Z.; Jiang, T.; Zhang, L.; Liu, B.; Wang, D.; Wang, L.; Xie, T. Surface treatment with Al^{3+} on a Ti-doped α-Fe_2O_3 nanorod array photoanode for efficient photoelectrochemical water splitting. *J. Mater. Chem. A* **2014**, *2*, 13705−13712.
(29) Hisatomi, T.; Le Formal, F.; Cornuz, M.; Brillet, J.; Tétreault, N.; Sivula, K.; Grätzel, M. Cathodic shift in onset potential of solar oxygen evolution on hematite by 13-group oxide overlayers. *Energy Environ. Sci.* **2011**, *4*, 2512−2515.
(30) Le Formal, F.; Tétreault, N.; Cornuz, M.; Moehl, Th.; Grätzel, M.; Sivula, K. Passivating surface states on water splitting hematite photoanodes with alumina overlayers. *Chem. Sci.* **2011**, *2*, 737−743.
(31) Xi, L.; et al. A Novel Strategy for Surface Treatment on Hematite Photoanode for Efficient Water Oxidation. *Chem. Sci.* **2013**, *4*, 164−169.
(32) Peter, L. M.; Wijayantha, K. G. U.; Tahir, A. A. Kinetics of Light-driven Oxygen Evolution at α-Fe_2O_3 Electrodes. *Faraday Discuss.* **2012**, *155*, 309−322.
(33) Le Formal, F.; Sivula, K.; Gratzel, M. The Transient Photocurrent and Photovoltage Behavior of a Hematite Photoanode under Working Conditions and the Influence of Surface Treatments. *J. Phys. Chem. C* **2012**, *116*, 26707−26720.
(34) Liu, R.; Zheng, Z.; Spurgeon, J.; Yang, X. Enhanced Photoelectrochemical Water-Splitting Performance of Semiconductors by Surface Passivation Layers. *Energy Environ. Sci.* **2014**, *7*, 2504−2517.
(35) Barroso, M.; Cowan, A. J.; Pendlebury, S. R.; Grätzel, M.; Klug, D. R.; Durrant, J. R. The Role of Cobalt Phosphate in Enhancing the Photocatalytic Activity of α-Fe_2O_3 toward Water Oxidation. *J. Am. Chem. Soc.* **2011**, *133*, 14868−14871.
(36) Iandolo, B.; Hellman, A. The Role of Surface States in the Oxygen Evolution Reaction on Hematite. *Angew. Chem., Int. Ed.* **2014**, *53*, 13404−13408.
(37) Barroso, M.; Mesa, C. A.; Pendlebury, S. R.; Cowan, A. J.; Hisatomi, T.; Sivula, K.; Grätzel, M.; Klug, D. R.; Durrant, J. R. Dynamics of photogenerated holes in surface modified a-Fe2O3 photoanodes for solar water splitting. *Proc. Natl. Acad. Sci. U. S. A.* **2012**, *109*, 15640−15645.
(38) Pendlebury, S. R.; et al. Correlating Long-lived Photogenerated Hole Populations with Photocurrent Densities in Hematite Water Oxidation Photoanodes. *Energy Environ. Sci.* **2012**, *5*, 6304−6312.
(39) Bluhm, H. Photoelectron Spectroscopy of Surfaces Under Humid Conditions. *J. Electron Spectrosc. Relat. Phenom.* **2010**, *177*, 71−84.
(40) Axnanda, S.; Crumlin, E. J.; Mao, B.; Rani, S.; Chang, R.; Karlsson, P. G.; Edwards, M. O. M.; Lundqvist, M.; Moberg, R.; Ross, P. N.; et al. Using "Tender" X-ray Ambient Pressure X-Ray Photoelectron Spectroscopy as a Direct Probe of Solid-Liquid Interface. *Sci. Rep.* **2015**, *5*, 9788.
(41) Ye, X.; Yang, J.; Boloor, M.; Melosh, N. A.; Chueh, W. C. Thermally-Enhanced Minority Carrier Collection in Hematite During Photoelectrochemical Water Splitting and Sulfite Oxidation. *J. Mater. Chem. A* **2015**, *3*, 10801−10810.
(42) Gerischer, H. The Impact of Semiconductors on the Concepts of Electrochemistry. *Electrochim. Acta* **1990**, *35*, 1677−1699.
(43) Lichterman, M. F.; Hu, S.; Richter, M. H.; Crumlin, E. J.; Axnanda, S.; Favaro, M.; Drisdell, W.; Hussain, Z.; Mayer, T.; Brunschwig, B. S.; et al. Direct Observation of the Energetics at a Semiconductor/Liquid Junction by *operando* X-ray Photoelectron Spectroscopy. *Energy Environ. Sci.* **2015**, *8*, 2409−2416.
(44) Nozik, A.; Memming, R. Physical Chemistry of Semiconductor−Liquid Interfaces. *J. Phys. Chem.* **1996**, *100*, 13061−13078.
(45) Sieber, K. D.; Sanchez, C.; Turner, J. E.; Somorjai, G. A. Prepartion, Characterisation and Photoelectronic properties of Germanium-substituted Fe_2O_3 Single Crystal. *J. Chem. Soc., Faraday Trans. 1* **1985**, *81*, 1263−1274.
(46) Duret, A.; Gratzel, M. Visible Light-Induced Water Oxidation on Mesoscopic α-Fe_2O_3 Films Made by Ultrasonic Spray Pyrolysis. *J. Phys. Chem. B* **2005**, *109*, 17184−17191.
(47) Karslioglu, O.; Nemšák, S.; Zegkinoglou, I.; Shavorskiy, A.; Hartl, M.; Salmassi, F.; Gullikson, E. M.; Ng, M. L.; Rameshan, Ch.; Rude, B.; et al. Aqueous Solution/Metal Interfaces Investigated *in operando* by Photoelectron Spectroscopy. *Faraday Discuss.* **2015**, *180*, 35−53.
(48) Favaro, M.; Jeong, B.; Ross, P. N.; Yano, J.; Hussain, Z.; Liu, Z.; Crumlin, E. J. Unravelling the Electrochemical Double Layer by Direct Probing of the Solid/Liquid Interface. *Nat. Commun.* **2016**, *7*, 12695.
(49) Long, P.; Sadeghi, H. R.; Rife, J. C.; Kabler, M. N. Surface Space-charge Dynamics and Surface Recombination on Silicon (111) Surfaces Measured with Combined Laser and Synchrotron Radiation. *Phys. Rev. Lett.* **1990**, *64*, 1158−1161.
(50) Zhang, A.; Yates, J. T. Band Bending in Semiconductors: Chemical and Physical Consequences at Surfaces and Interfaces. *Chem. Rev.* **2012**, *112*, 5520−5551.
(51) Gerischer, H. Electrolytic Decomposition and Photodecomposition of Compound Semiconductors in Contact with Electrolytes. *J. Vac. Sci. Technol.* **1978**, *15*, 1422−1428.
(52) Chen, S.; Wang, L.-W. Thermodynamic Oxidation and Reduction Potentials of Photocatalytic Semiconductors in Aqueous Solution. *Chem. Mater.* **2012**, *24*, 3659−3666.
(53) Frese, K. W.; Madou, M. J.; Morrison, S. R. Investigation of Photoelectrochemical Corrosion of Semiconductors. *J. Phys. Chem.* **1980**, *84*, 3172−3178.
(54) Allongue, P.; Blonkowski, S. Corrosion of III-V Compounds; A Comparative Study of GaAs and InP: Part I. Electrochemical Characterization Based on Tafel Plot Measurements. *J. Electroanal. Chem. Interfacial Electrochem.* **1991**, *316*, 57−77.
(55) Emfietzoglou, D.; Nikjoo, H. Accurate Electron Inelastic Cross Sections and Stopping Powers for Liquid Water over the 0.1−10 keV Range Based on an Improved Dielectric Description of the Bethe Surface. *Radiat. Res.* **2007**, *167*, 110−120.

DOI: 10.1021/acs.jpclett.7b02548
J. Phys. Chem. Lett. 2017, 8, 5579−5586